3-D Magnetotelluric Image of Offshore Magmatism at the Walvis Ridge and Rift Basin

Marion Jegen[1], Anna Avdeeva[1,2], Christian Berndt[1], Gesa Franz[1], Björn Heincke[1,3], Sebastian Hölz[1], Anne Neska[4], Anna Marti[5], Lars Planert[1,6], J. Chen[1,], Heidrun Kopp[1], Kiyoshi Baba[7] , Oliver Ritter[8], Ute Weckmann[8], Naser Meqbel[8] and Jan Behrmann[1].

[1]Geomar, Helmholtz Centre for Ocean Research, Wischhofstr. 1-3, 24148 Kiel, Germany
[2]now at University of Leicester, University Road, Leicester LE1 7RH, United Kingdom
[3]now at GEUS, Øster Voldgade 1, 1350 Copenhagen, Denmark
[4]Institute of Geophysics, Polish Academy of Science, ul. Księcia Janusza 64, 01452 Warsaw, Poland
[5]University of Barcelona, C. Marti I Franques, 08028 Barcelona, Spain
[6]now at Forschungsanstalt für Wasserschall und Geophysik, WTD71, Klausdorfer Weg 2, D-24148 Kiel, Germany
[7]Earthquake Research Institute, The University of Tokyo, 1-1-1 Yayoi, Bunkyo-ku, Tokyo 113-0032, Japan
[8]GFZ German Research Centre for Geosciences, Telegrafenberg 14473, Potsdam, Germany

1. Abstract

The Namibian continental margin marks the starting point of the Tristan da Cunha hotspot trail, the Walvis Ridge. This section of the volcanic southwestern African margin is therefore ideal to study the interaction of hotspot volcanism and rifting, which occurred in the late Jurassic/early Cretaceous. Offshore magnetotelluric data image electromagnetically the landfall of Walvis Ridge. Two large-scale high resistivity anomalies in the 3-D resistivity model indicate old magmatic intrusions related to hot-spot volcanism and rifting. The large-scale resistivity anomalies correlate with seismically identified lower crustal high velocity anomalies attributed to magmatic underplating along 2-D offshore seismic profiles. One of the high resistivity anomalies (above 500 Ωm) has three arms of approximately 100 km width and 300 km to 400 km length at 120 degree angles in the lower crust. One of the arms stretches underneath Walvis Ridge. The shape is suggestive of crustal extension due to local uplift. It might indicate the location where the hot-spot impinged on the crust prior to rifting. A second, smaller anomaly of 50 km width underneath the continent ocean boundary may be attributed to magma ascent during rifting. We attribute a low resistivity anomaly east of the continent ocean boundary and south of Walvis Ridge to

the presence of a rift basin that formed prior to the rifting.

2. Introduction

Passive margins bordering the South Atlantic oceanic basin were active during the Late Jurassic and Early Cretaceous when Western Gondwana ruptured and the South Atlantic Ocean opened from south to north (Light et al., 1993; Macdonald et al., 2003). These margins offer a unique opportunity to study ancient geological processes linking magmatism, continental extension, crustal breakup and subsidence during and after rifting.

The South Atlantic passive margins can be grouped into three provinces based on crustal structure and bathymetric expression: (1) *The province south of Walvis Ridge, offshore northern Namibia and south of the Florianopolis Basement High and Rio Grande Rise offshore southern Brazil.* Here, magmatism was voluminous, and formed volcanic wedges broader than 100 km within the crust (Franke et al., 2007). These wedges are manifested as seaward dipping reflectors (SDR) in seismic reflection sections on the conjugate Namibian (Elliott et al., 2009; Gladczenko et al., 1998) and Argentine margins (Franke et al., 2007). (2) *The province adjacent to Walvis Ridge and Rio Grande Rise.* These parts of both margins are dominated by magmatism, with its continental extensions into the Paraná Basalt Province and the Etendeka Plateau attesting to possible activity of the Tristan da Cunha hot spot (O'Connor and Duncan, 1990). (3) *The province north of Walvis Ridge and Rio Grande Rise, the margin of eastern Brazil and the counterpart offshore Congo and Angola.* These margins also experienced volcanism during break up, but syn-rift and early post-rift evolution was dominated by the formation of Aptian salt, shallow water carbonates, and clastic sediments.

Shore line crossing geophysical and geological experiments have been carried out in the Namibian central province at the landfall of Walvis Ridge within the framework of the priority program SPP1375 SAMPLE: South Atlantic Margin Processes and Links with onshore Evolution project. The ridge constitutes the bathymetric expression of the interaction of the Tristan da Cunha hot spot with the opening of the South Atlantic through a 1,500 km long bathymetric high of up to 2,000 m with a strike direction of NE-SW. To the north, the ridge bathymetry sharply terminates against the Florianopolis fracture zone (FFZ) (Sibuet et al., 1984). Seismically imaged

Moho shows that thickened oceanic crust underlies Walvis Ridge, whereas the oceanic crust north of the fracture zone is much thinner (Fromm et al., 2015). It has been suggested that the crust, which initially formed to the north of Walvis Ridge, has been sheared through an eastward ridge jump in the initial opening phase along the FFZ and transferred to the South American margin as the Sao Paolo Plateau (Sibuet et al., 1984), but there is no conclusive geophysical evidence for this and this ridge jump is not included in the newest plate reconstructions for the South Atlantic (Seton et al., 2012). Walvis Ridge itself is underlain by a lower crustal high velocity anomaly from landfall over a length of approximately 300 km (Fromm et al., 2015), which may be attributed to underplating related to the Tristan da Cunha hot spot. Onshore underplating has been documented by high seismic v_p/v_s ratios (> 1.8) and thickened oceanic crust at the northern end of the landfall (Heit et al., 2015) and as a zone of increased v_p velocity (> 7.5 km/s) of approximately 100 km width beneath the landfall of Walvis Ridge (Ryberg et al., 2015). The Tristan da Cunha plume gave rise to only a small hot-spot, i.e. plume surface expression on the seafloor, based on these seismic studies.

However velocity models on land are sparse and offshore only 2-D seismic profiles exist. In order to better assess the region of impact coherently over a regional scale, we carried out a magnetotelluric (MT) experiment to derive a regional 3-D resistivity model. Comparison of the large-scale resistivity image to regional seismic models and a density model based on satellite data and seismic information (Maystrenko et al., 2013) provides additional constraints on magmatism. Based on this resistivity model we analyze the rifting sequence and magmatic evolution of Walvis Ridge on a regional scale and further constrain the link between the Tristan da Cunha hotspot and the opening of the South Atlantic.

3. Marine MT experiment

Electrical conduction in rocks is dominated by ionic conduction within pore fluids (typically water or partial melt), leading to a first order dependence of bulk resistivity on the amount of pore fluid within the rock matrix. A less common conducting mechanism occurs along particular electrically conductive minerals such as graphite

98 or metal containing minerals (Palacky, 1987; Keller, 1987). Both conducting
99 mechanisms are dependent on temperature.

100 Dry rocks with low porosity such as old deep volcanic intrusions have increased
101 resistivity (Kariya and Shankland, 1983; Shankland and Ander, 1983; Palacky, 1987),
102 sediments with larger fluid filled pore fraction have a lower resistivity. Metamorphic
103 rocks have an even lower resistivity if they contain graphite or other electrically
104 conducting minerals. Shear zones are for example often associated with low electrical
105 resistivity due to the fact that they either act as pathways of fluids or contain graphite.

106 The MT method is an electromagnetic method that uses natural variations of the
107 Earth's magnetic field as an electromagnetic source. It has first been proposed by
108 Cagniard (1953) and has been discussed in a variety of textbooks, most recently by
109 Chave and Jones (2013). The MT impedance is the Earth's response to this natural
110 electromagnetic source and represents resistivity variations within the Earth. The
111 impedance is a complex valued matrix with four elements and is derived from
112 measurements of orthogonal electric and orthogonal magnetic field variations. The
113 elements of the impedance matrix are related to the ratio of horizontal electric and
114 magnetic field variations along the two coordinate axes at a particular period.
115 Impedance values at increasing periods contain information about resistivity
116 structures at increasing depth. As opposed to active source seismic data and similar to
117 potential field data, the MT data are not only sensitive to the region within the
118 measurement array, but also influenced by electrical resistivity variations beyond the
119 array of sites. The sensitivity to resistivity variations beyond the measurement array
120 decreases with increasing distance from the array and decreasing period. A resistivity
121 structure of the subsurface is derived in a final step from the data via inversion.

122 For the MT experiment in Namibia we acquired data offshore along two orthogonal
123 profiles, one parallel and one perpendicular to Walvis Ridge (Figure 1). Along these
124 profiles we occupied 45 sites in total with a spacing of approximately 10 km apart.
125 The profile orthogonal to Walvis Ridge ran along the ocean continent boundary, the
126 profile along Walvis Ridge placed in line with the land profiles along one of the few
127 roads in this region leading into the continent. The offshore data were acquired during
128 two deployments and recoveries on RV Maria S. Merian cruises MSM 17-1 and MSM
129 17-2 with ocean bottom electromagnetic (OBEM) instruments developed at

GEOMAR. The bottom time of the OBEM instruments was around 3 weeks, with continuous recordings at a sampling rate of 1 Hz of two orthogonal horizontal electric fields and three orthogonal magnetic fields (using a three component fluxgate magnetometer) as well as tilt and temperature readings. The offshore data were complemented with a subset of seven onshore stations with 5-component (two orthogonal electric and 3 orthogonal magnetic) broadband MT instruments (10 kHz – 1 mHz) from a land MT grid run by GFZ Potsdam (Kapinos et al., 2016). These coastal sites were essential for the derivation of the 3-D resistivity model since the data contain information about the strong conductivity contrast at the Namibian coast. The electromagnetic coast effect causes a particularly strong distortion at the coast. If this boundary is not constrained by data on both sides or through a good priori conductivity model on the opposing site of the array, it can lead to a strongly distorted resistivity model (Worzewski et al., 2012).

From the acquired offshore data, only data from 32 out of 45 sites could be used for further analysis. At 13 sites, either loss of data on some channels, lack of time synchronization or electronic noise on the electric field channels prevented further analysis.

The processing of the data to compute the impedance as a function of period consists of several steps: First we corrected the electric and magnetic field variations for instrument tilt and then we rotated the data to a single coordinate system (x, y, z pointing northward, eastward and downwards, respectively). To calculate the impedance from our time series, we used the bounded influence algorithm (Chave and Thomson, 2004) and the multi-station scheme (Egbert, 1997). We obtained the impedance tensors for frequencies ranging from 0.1 Hz to 10^{-4} Hz for the offshore data. Examples of the complex valued impedance, expressed as apparent resistivity and phase for all four elements of the impedance matrix as a function of period are displayed in Figure 2. We show observed data for stations at which the data demonstrate both high (sites 23, 26 and 4) and moderate quality data (site 6).

The magnetotelluric impedance matrix contains information about whether the variations in the subsurface electrical resistivity sensed by the data are predominantly 1-D, 2-D or 3-D. Based on a dimensionality analysis described by Marti et al. (2009), we observe that the data has a clear 3-D character at almost all sites. The 3-D

resistivity variations seen in the data can be attributed to the rough topography (topographic high of Walvis Ridge running roughly orthogonal to the strong resistivity contrast across the coast) and 3-D resistivity variations within the seafloor. We therefore inverted the data to find a 3D resistivity model, taking into consideration the complex seafloor bathymetry. although the experiment was originally set up for two 2D profiles. Since MT data is sensitive to resistivity variations well beyond the site location (especially for large period datasets as in this study), the error introduced in the derived 3D model through the unequal site distribution across the survey area is smaller than neglecting the complex and pronounced 3D bathymetry. The model derived here is therefore more complete than the initial 2-D model presented by Kapinos et al. (2016) based on an amphibious profile containing the offshore data along profile 1.

A 3-D resistivity model of the Walvis Ridge area was obtained using a 3-D MT inversion code (Avdeeva et al., 2012; Moorkamp et al., 2010). The code allows positioning of MT sites at the seafloor and inclusion of bathymetry. The bathymetry was approximated with a rectilinear mesh where horizontal cell sizes are constant throughout the whole 3-D inversion volume. In addition, the modeling mesh is embedded in a 1-D layered background. In our case, the volume of interest covers the ocean in the west and continental crust to the east, such that a single 1-D background model is inadequate. To overcome this problem, we extended the inversion mesh to the sides so that the influence of a single 1D background model, inadequately representing both the ocean- and land-side of the model simultaneously, is negligible.

There is a tradeoff between available computational resources and the accuracy of the inverse problem solution. The mesh has to be fine enough to approximate the bathymetry of the seafloor and to achieve accurate solutions for smaller period data, yet not so large that computation time and memory requirements become unrealistic. The mesh must also match the survey geometry and resolution of the MT method, i.e. horizontal discretization should not be much smaller than the distance between adjacent sites. Due to failure to recover data at some stations, the spacing is as large as 60 km in some regions. Taking all these considerations into account, we chose a mesh consisting of 96×92×34 cells and covering an area of 960×920×300 km^3. The horizontal dimensions of the cells are 10 km, while the vertical cell sizes are increasing with depth from 100 m to 50 km.

The starting model included the Atlantic Ocean (0.3 Ωm) and a crude bathymetry of Walvis Ridge with a 1 Ωm sediment layer. If we do not include a sediment layer in the starting model the inversion does not converge. Below the sediments the model consists of a homogeneous half-space. We ran numerous inversions varying the thicknesses of the sedimentary layer and resistivity of the initial half-space while considering different data weights, error floors, and regularization strategies. Here, we present our inversion result, which based on our testing, delivers the most credible results. For this inversion run we started with a 3 km sediment layer with a 500 Ωm half-space below. We used smooth regularization, with a regularization functional based on a gradient operator, and adopt a cooling strategy for choosing the regularization parameters. This means that during the first stages of the inversion we require smooth resistivity models. This constraint is then gradually relaxed. We furthermore assume a typical error floor of 5% in the impedance data. Due to the fact that the starting model already contains the ocean, sediments, and a crude approximation of the bathymetry, the modeled impedance due to this starting model, termed initial data, fits the observed data with a relatively low RMS misfit of 5.6. The inversion of this starting model to our final model produces modeled data, termed predicted data, with an RMS misfit of 2.27. The misfit could not be reduced any further, which we attribute to the relatively coarse bathymetry approximation with a rectilinear mesh.

A comparison of initial and predicted data with the observed apparent resistivities and phases is shown in Figure 2 for exemplary individual sites. The inversion significantly improves the data fit compared to the predicted data of the initial model. An overall comparison of predicted and observed data for the off-diagonal elements of the impedance is shown in Figure 3 in the form of pseudo sections of apparent resistivity and phase as a function of period.

In order to validate the resistivity model obtained by the inversion, RMS values for individual sites and periods are shown in Figure 4. For most sites and periods the RMS value is below 3. The predicted data for sites 1, 2, 23, 25 and 45, all of which are located at the end of the profiles, do not show a satisfactory fit to the observed data. These sites, but for site 25, are located at the deepest parts of the profiles offshore, where signal to noise ratio is smallest due to increased absorption of electromagnetic energy by the overlying conductive ocean. Furthermore the vertical

grid size, which increases with depth, might be too large at these stations to model the underlying subsurface resistivity variations in the upper part of the model or changes of bathymetry occurring in the region. This would explain why the increased misfit is particularly strong at smaller periods. Very good data fits observed for sites 6 and 19 should be attributed to the fact that the data quality at these sites was very poor (see site 6 in Figure 2) and as a consequence data errors large.

4. Results

We present our resistivity model as five horizontal slices for depths of 8.5 km-10 km, 12.5 km -15km, 15 km - 20 km, 25 km - 30 km and 42.5 km - 50 km shown in Figure 5. On these horizontal slices, the coastline is superimposed as a black line. The Etendeka flood basalt regions are shown as textured areas. Other main geological features are shown as white lines and have been derived from seismic transects 1 to 4 in Gladczenko et al. (1998). The locations of these transects are marked by black lines. The seismically inferred continent-ocean boundary (COB) is shown as a solid line and is defined as the western termination of the lowermost seaward dipping reflector. Gladczenko et al. (1998) inferred that a late Jurassic- early Cretaceous rift basin (JCR) formed prior to the break up. The dashed line marks its eastern limit based on seismic data.

Before we discuss the particular features of the resistivity model, we would like to point out that the model is not equally well resolved everywhere. As discussed in the previous section, MT data is generally sensitive to resistivities beyond the array, but resolution decreases with increasing distance. We therefore consider small-scale variations on the continent east of our land stations as not well resolved. A land data set (see Kapinos et al., 2016 for station lay out) is currently being analysed through a 3-D inversion and will probably give a higher resolution image of this area. The land data also contain short period data, which will allow the derivation of higher resolution models in the upper crust.

The shallowest slice through our model is characterized by a number of smaller scale anomalies. They mainly occur in the vicinity of sites where the predicted and observed short period data exhibit a large misfit (Figure 4). Our relatively coarse gridding of the model cannot reliably invert for these anomalies and we do not consider them in the further discussion.

On the other hand, two large-scale resistivity anomalies north (high resistivity, marked as R1 in Figure 5) and south (low resistivity, marked as C in Figure 5) of Walvis Ridge are well resolved. The resistive anomaly R1 persists through all depth slices, and extends further underneath Walvis Ridge and along a region south of Walvis Ridge underneath the coast with increasing depth. It can therefore be regarded as a large-scale, crustal/upper lithospheric mantle anomaly. At depths below 15 km, a second region of high resistivity (R2 in Figure 5) underneath the COB south of Walvis Ridge appears, which persists down to the base of our model.

The low resistivity feature also persists through all depth slices. However, the sensitivity of MT data is reduced beneath conducting regions. Sensitivity studies have shown that the model in this region is resolved well down to a depth of approximately 25 km. We have therefore blended out the low resistivity zone in the two lowermost slices of our model.

For the discussion of the current inversion model we will concentrate on these main large-scale features. In order to determine their tectonic origin, we will compare the resistivity features to other geophysical data from the region, i.e. mainly offshore seismic data. For the discussion of the resistive region on land, we will furthermore compare the results to a density model, which has been derived by Maystrenko et al. (2013) and which partly overlaps our study region. After verification of our model with these data sets, we will interpret the observed spatial pattern in terms of their tectonic-magmatic implication for the opening of the South Atlantic.

High resistivity zone R1 (Magmatic Intrusions Walvis Ridge and Coast):

MT data are generally not very sensitive to the precise resistivity value within a resistive feature. While the data require a resistivity contrast to the surrounding model in the area shaded in dark blue representative of resistivities above 1,000 Ωm (Figure 5), models where this region is changed to values of down to 500 Ωm fit the data equally well.

The outline of the offshore high resistivity zone at depths of 25 km - 30 km and 42.5 km - 50 km correlates with a region of high seismic velocity anomalies in the lower crust detected along co-occupied seismic refraction lines along the offshore MT profiles (P3 and P100) as well as by a seismic line trending from the Angola basin over the landfall of Walvis Ridge to the onshore domain (P2). The widths, where

292 increased lower crustal velocities have been detected along these profiles by Fromm
293 et al. (2015) are marked in orange in Figure 5 in our model slices at lower crustal
294 depth. The lower crustal high velocity region is interpreted as magmatic underplating
295 and has been attributed Fromm et al. (2015) as the region that has been affected by the
296 mantle plume. We therefore presume that the high resistive zone delineates the region,
297 where the ascending mantle plume from depth has imprinted the crust and lithospheric
298 mantle. Further evidence supporting our interpretation of the high resistivity zone on
299 land, where our model has arguably less resolution, comes from land studies. Heit et
300 al. (2015) report a strong increase in crustal thickness to 44 km and high seismic v_p/v_s
301 ratios of 1.89 on the African continent at the landfall of Walvis Ridge and northeast of
302 the landfall. Ryberg et al. (2015) detect increased lower crustal compressional
303 velocities above 7.5 km/s at the landfall of Walvis Ridge. Both authors attribute the
304 observations to magmatic underplating produced by the mantle plume during the
305 breakup of Gondwana. A gravity model (Maystrenko et al., 2013) of the South-
306 African margin overlaps up to about 17.5°S with our model, supplying spatial
307 information on the thickness of the continental crust within the longitudes of 9°E and
308 20°E for Walvis Ridge and the region south of Walvis Ridge. The study identifies a
309 lower crustal high-density body with densities of 2.95 kg/m^3 (outlined in pink in
310 Figure 5 for our horizontal slices below 25 km), which coincides with the continental
311 part of our resistor.

312 At depths above 25 km some of the outer regions of the high resistivity anomaly R1 in
313 our model are replaced by decreasing resistivities indicative of higher porosity
314 perhaps due to more severe weathering of extrusive volcanic rocks (Planke and
315 Alvestad, 1999).

316 Based on the spatial coincidence of our resistivity anomaly and high lower crustal
317 velocities that were interpreted as magmatic underplating, we interpret the highly
318 resistive anomaly (R1 in Figure 5) as the region where magma has risen from the
319 mantle into the crust. We suggest that the anomaly delineates the extent of the Tristan
320 da Cunha plume impact.

321 **Low resistivity zone C (Rift Basin):**
322 While the boundary to the north of the resistivity anomaly R1 is diffuse, the southern
323 edge is characterized by an abrupt change towards low resistivities (anomaly C), just

south of our profile line along Walvis Ridge. Within the upper 10 km, the electrical resistivity model exhibits a gradual change from a very low resistivity region in the far east (< 3 Ωm) to intermediate resistivities of less than 10 Ωm to approximately 10 to 100 Ωm towards the COB. Comparison of the resistivity model with seismic results along transect 2 and 3 (Figure 6) suggests that the likely cause of these low resistivities is the presence of the rift basin that formed prior to the breakup of Gondwana (Gladczenko et al., 1998). The region with resistivities of about 3 to 10 Ωm coincides with this Jurassic Cretaceous rift basin (JCR). Very low resistivities are found in the area east of the boundary that separates the JCR from the old continental belt. Within this region the seismic transects exhibit reflectors, which have been interpreted as Late Precambrian shear zones (Clemson et al., 1997; Light et al., 1993), or thrusts reactivated as Late Mesozoic extensional faults (Gladczenko et al., 1998). Metamorphic minerals or potentially small amounts of graphite in the shear zone may explain the extremely low resistivities (Haak and Hutton, 1986).

The lack of a rift basin north of Walvis Ridge may be due to an eastward relocation of rifting and magmatism north of Walvis Ridge. This relocation may have sheared off parts of the northern rift basin and its seaward dipping reflectors to the South-American side along the Floreanopolis Fracture Zone (Sibuet et al., 1984; Elliot and Berndt, 2009).

High resistivity zone R2 (Magmatism related to rifting along COB)

In the region below 10 km depth, west of the COB, we observe an increase of resistivity in a band of approximately 100 km in which resistivities as high as several 100 Ωm (anomaly R2, Figure 6) are observed, which point to magmatic intrusions related to the rifting and break up. The overlying extrusive basalt flows obscure deep seismic reflections in this region and thus a seismic verification of the magmatic intrusions, but for other volcanic rifted margins it has been shown that the seaward dipping reflectors are frequently underlain by magmatic intrusions (Skogseid and Eldholm, 1987). In terms of electrical resistivity, the overlying extrusive basalt flows do not constitute a high resistivity anomaly, but exhibit resistivity in the range of tens of Ωm to 100 Ωm. This value is typical for extrusive basalt layers in rifted margins (Jegen et al., 2009).

East of the COB, seismic data indicate the presence of a high velocity lower crustal body at a depth below 25 km. Our data show no indication of a high resistivity zone in this region, which may be due to decreased sensitivity underneath the conductive upper crust in this region. For further comparison, we have plotted the base of the sediment within the JCR, the top of the high velocity body and the Moho as inferred from gravimetric data (Maystrenko et al., 2013) in Figure 6. On the western, oceanic part of the section the top of the lithospheric high resistivity region coincides with the top of the lower crustal high velocity zone. East of the COB, the anomalous deep crustal bodies derived from gravity and seismic data do not match, showing the limitations of these crustal models.

5. Discussion: Implications for tectono-magmatic processes during the formation of the Namibia volcanic rifted margin

The magnetotelluric data provide two additional constraints on the deep crustal structure that were not known from seismic studies before. The highly resistive zone underlying both the Walvis Ridge (also shown in the 2D model by Kapinos et al. (2016) and the seaward dipping reflectors south of it (anomalies R1 and R2) coincide with the bulk of the extrusive volcanic material encountered on the Namibian margin.

Near the coast the R1 anomaly consists of three arms protruding to the north along the coastline, to the WSW along the Walvis Ridge, and to the SSE towards the Etendeka flood basalt province (Figure 7). This 120 degree-spread between rift arms is typical for point sources impinging into the crust, e.g. the rift arms of a shield volcano or the ridge-ridge-ridge triple junction of the Afar hotspot, and we interpret the high resistivity anomaly as the effect of the Tristan da Cunha hotspot where it impinged the lithosphere at about 133 Ma (Müller et al., 1993) as shown in Figure 7a. Based on our resistivity model, we would therefore place the Tristan da Cunha hotspot on the African plate as suggested by Thompson and Gibson (1991) and Harry and Sawyer (1992) and not on the South American plate as favored by O'Connor and Duncan, (1990) and Turner et al. (1994).

After the short and vigorous continental flood basalt emplacement the plume manifested itself in break-up volcanism with its center underneath the Walvis Ridge

but additional strong magma supply along the incipient break-up axis to the south (Figure 7b). We interpret the resistive zone R2 that stretches south from the Walvis Ridge underneath the center of the seaward dipping reflectors (along the COB) as the magma conduits that fueled the volcanism leading to the emplacement of the seaward dipping reflectors during the rifting stage and break-up stage. The resistivities here are lower than those in the area of seismically imaged underplating farther north but larger than those underneath the normal oceanic crust farther west. The sedimentary basin and in particular the old rifted continental crust between the JCR and the coast line show low resistivities that are considerably lower than normal continental crust.

6. Conclusion

In this study we present a 3-D resistivity model derived from a large-scale offshore experiment that was augmented by seven coastal land stations. The resistivity model reaching into the lithosphere maps the regions of increased magmatic production through the Tristan da Cunha mantle plume and rifting, as comparison with other available geophysical data in the area shows. The scale of the 3-D resistivity model connects the piece-wise offshore information in form of 2-D seismic profiles with onshore geology and provides valuable insight in the spatial distribution of increased magmatic activity. The big high resistivity anomaly with three arms might represent the rift arms that are expected to occur when the lithosphere is uplifted by a mantle plume. The narrow resistive zone striking along the COB, west of the low resistivity rift basin, is most likely related to magmatism during the break up of the continent.

The regional extent of the offshore 3-D experiment presented here and by Baba et al (this issue) is one of the largest-scale academic offshore experiment of this type performed up to now, next to a recent study in the Alboran Sea (Garcia et al., 2015). While the current model shows some encouraging results and we are confident about the larger scale features, the methodology and inversion algorithms may be further improved in terms of resolution of the inversion model in the upper region. The large orthogonal topography variations due to Walvis ridge and the coast make rectilinear meshes not optimal as a large portion of the computationally feasible grid is used up for representing the topography.

Acknowledgements

We thank the captain and the crew of R/V Maria S. Merian for the professional and friendly support of the scientific work in the cruises. This work was supported by the German Research Foundation (DFG) as part of the Priority Program SPP1375 and the Future Ocean program of Kiel Marine Sciences. The computations were performed using the ALICE High Performance Computing Facility at the University of Leicester.

7. References

Avdeeva, A., Avdeev, D., Jegen, M., 2012. Detecting a salt dome overhang with magnetotellurics: 3D inversion methodology and synthetic model studies. GEOPHYSICS 77, E251–E263. doi:10.1190/geo2011-0167.1

Cagniard L.,1953. Basic theory of the magnetotelluric method of geophysical prospecting, Geophysics, 18, 605–635.

Chave, A.D. and Jones G. A., 2013. The Magnetotelluric Method, Theory and Practice, Cambridge University Press, ISBN 9780521819275.

Chave, A.D., Thomson, D.J., 2004. Bounded influence magnetotelluric response function estimation. Geophysical Journal International 157, 988–1006. doi:10.1111/j.1365-246X.2004.02203.x

Clemson, J., Cartwright, J., BOOTH, J., 1997. Structural segmentation and the influence of basement structure on the Namibian passive margin. Journal of the Geological Society 154, 477–482. doi:10.1144/gsjgs.154.3.0477

Coffin, M.F., Eldholm, O., 1994. Large Igneous Provinces: crustal structure, dimensions, and external consequences. Rev. Geophys. 32, 1–36.

Egbert, G.D., 1997. Robust multiple-station magnetotelluric data processing. Geophysical Journal International 130, 475–496. doi:10.1111/j.1365-246X.1997.tb05663.x

Elliott, G.M., Berndt, C., Parson, L.M., 2009. The SW African volcanic rifted margin and the initiation of the Walvis Ridge, South Atlantic. Mar Geophys Res 30, 207–214. doi:10.1007/s11001-009-9077-x

Franke, D., Neben, S., Ladage, S., Schreckenberger, B., Hinz, K., 2007. Margin segmentation and volcano-tectonic architecture along the volcanic margin off Argentina/Uruguay, South Atlantic. Marine Geology 244, 46–67. doi:10.1016/j.margeo.2007.06.009

Fromm, T., Planert, L., Jokat, W., Ryberg, T., Behrmann, J.H., Weber, M.H., Haberland, C., 2015. South Atlantic opening: A plume-induced breakup? Geology 43, 931–934. doi:10.1130/G36936.1

Garcia, X., Seillé, H., Elsenbeck, J., Evans, R.L., Jegen, M., Hölz, S., Ledo, J., Lovatini, A., Martí, A., Marcuello, A., Queralt, P., Ungarelli, C., Ranero, C.R., 2015. Structure of the mantle beneath the Alboran Basin from magnetotelluric soundings. Geochem. Geophys. Geosyst. 16, 4261–4274. doi:10.1002/2015GC006100

Gladczenko, T.P., Skogseid, J., Eldholm, O., 1998. Namibia volcanic margin. Mar Geophys Res 20, 313–341.

Haak, V., Hutton, R., 1986. Electrical resistivity in continental lower crust. Geological Society, London, Special Publications 24, 35–49. doi:10.1144/GSL.SP.1986.024.01.05

Harry, D.L., Sawyer, D.S., 1992. Basaltic volcanism, mantle plumes, and the

466 mechanics of rifting: The Paraná flood basalt province of South America.
467 Geology 20, 207–210.
468 Heit, B., Yuan, X., Weber, M., Geissler, W., Jokat, W., Lushetile, B., Hoffmann, K.-H.,
469 2015. Crustal thickness and V p/ V sratio in NW Namibia from receiver
470 functions: Evidence for magmatic underplating due to mantle plume-crust
471 interaction. Geophys. Res. Lett. 42, 3330–3337. doi:10.1002/2015GL063704
472 Jegen, M.D., Hobbs, R.W., Tarits, P., Chave, A., 2009. Joint inversion of marine
473 magnetotelluric and gravity data incorporating seismic
474 constraintsPreliminary results of sub-basalt imaging off the Faroe Shelf.
475 Earth and Planetary Science Letters 282, 47–55.
476 doi:10.1016/j.epsl.2009.02.018
477 Kapinos, G., Weckmann, U., Jegen-Kulcsar, M., Meqbel, N., Neska, A., Katjiuongua,
478 T.T., Hoelz, S., Ritter, O., 2016. Electrical resistivity image of the South
479 Atlantic continental margin derived from onshore and offshore
480 magnetotelluric data. Geophys. Res. Lett. 43, 154–160.
481 doi:10.1002/2015GL066811
482 Kariya, K.A. and Shankland, T. J., 1983. Electrical conductivity of dry lower crustal
483 rocks, Geophysics, 48, 52-61.
484 Keller, G.V., 1987. Rock and mineral properties, in Nabighian, M.N., ed.,
485 Electromagnetic Methods in Applied Geophysics, Volume 1, Theory: Tulsa
486 Oklahoma, Society of Exploration Geophysicists, p. 13-51.
487 Light, M.P.R., Maslanyj, M.P., Greenwood, R.J., Banks, N.L., 1993. Seismic sequence
488 stratigraphy and tectonics offshore Namibia, in: Tectonics and Seismic
489 Sequence Stratigraphy. Geological Society, London, pp. 163–191.
490 Macdonald, D., Gomez-Perez, I., Franzese, J., Spalletti, L., Lawver, L., Gahagan, L.,
491 Dalziel, I., Thomas, C., Trewin, N., Hole, M., Paton, D., 2003. Mesozoic break-
492 up of SW Gondwana: implications for regional hydrocarbon potential of the
493 southern South Atlantic. Marine and Petroleum Geology 20, 287–308.
494 doi:10.1016/S0264-8172(03)00045-X
495 Martí, A., Queralt, P., Ledo, J., 2009. WALDIM: A code for the dimensionality
496 analysis of magnetotelluric data using the rotational invariants of the
497 magnetotelluric tensor. Computers & Geosciences, 35, 2295–2303.
498 doi:10.1016/j.cageo.2009.03.004
499 Maystrenko, Y.P., Scheck-Wenderoth, M., Hartwig, A., Anka, Z., Watts, A.B., Hirsch,
500 K.K., Fishwick, S., 2013. Structural features of the Southwest African
501 continental margin according to results of lithosphere-scale 3D gravity and
502 thermal modelling. Tectonophysics 604, 104–121.
503 doi:10.1016/j.tecto.2013.04.014
504 Moorkamp, M., Heincke, B., Jegen, M., Roberts, A.W., Hobbs, R.W., 2010. A
505 framework for 3-D joint inversion of MT, gravity and seismic refraction data.
506 Geophysical Journal International 184, 477–493. doi:10.1111/j.1365-
507 246X.2010.04856.x
508 Müller, R.D., Royer, J.-Y., Lawver, L.A., 1993. Revised plate motions relative to the
509 hotspots from combined Atlantic and Indian Ocean hotspot tracks. Geology
510 21, 275–278.
511 O'Connor, J.M., Duncan, R.A., 1990. Evolution of the Walvis Ridge-Rio Grande Rise
512 Hot Spot System: Implications for African and South American Plate motions
513 over plumes. J. Geophys. Res. Solid Earth 95, 17475–17502.
514 doi:10.1029/JB095iB11p17475

Palacky, G.J., 1987. Resistivity characterization of geologic targets, in Nabighian, M.N., ed., Electromagnetic Methods in Applied Geophysics, Volume 1, Theory: Tulsa Oklahoma, Society of Exploration Geophysicists, 53-129.

Planke, S., Alvestad, E. 1999. Seismic volcanostratigraphy of the extrusive breakup complexes in the northeast Atlantic: implications from ODP/DSDP drilling, Proc. Ocean Drill. Program Sci. Results, 163, 1-16.

Ryberg, T., Haberland, C., Haberlau, T., Weber, M.H., Bauer, K., Behrmann, J.H., Jokat, W., 2015. Crustal structure of northwest Namibia: Evidence for plume-rift-continent interaction. Geology 43, 739–742. doi:10.1130/G36768.1

Seton, M., Müller, R.D., Zahirovic, S., Gaina, C., TORSVIK, T., Shephard, G., Talsma, A., Gurnis, M., Turner, M., Maus, S., Chandler, M., 2012. Global continental and ocean basin reconstructions since 200Ma. Earth-Science Reviews 113, 212–270. doi:10.1016/j.earscirev.2012.03.002

Shankland, T.J. and Ander M.E., 1983. Electrical Conductivity, Temperature , and Fluids in the Lower Crust. Journal of Geophysical Research, Vol. 88, B11, 9475-9484.

Sibuet, J.C., Hay, W.W., Prunier, A., Montadert, L., Hinz, K., Fritsch, J., 1984. The Eastern Walvis Ridge and Adjacent Basins (South Atlantic): Morphology, Stratigraphy, and Structural Evolution in Light of the Results of Legs 40 and 75, in: Initial Reports of the Deep Sea Drilling Project, 75, Initial Reports of the Deep Sea Drilling Project. U.S. Government Printing Office. doi:10.2973/dsdp.proc.75.108.1984

Skogseid, J., Eldholm, O., 1987. Early Cenozoic crust at the Norwegian continental margin and conjugate Jan Mayen Ridge. J. Geophys. Res. 92, 11,471–11,491.

Thompson, R.N., Gibson, S.A., 1991. Subcontinental mantle plumes, hotspots and pre-existing thinspots. Journal of the Geological Society 148, 973–977.

Turner, S., Regelous, M., Kelley, S., Hawkesworth, C., Mantowani, M., 1994. Magmatism and continental break-up in the South Atlantic: high precision 40Ar-39Ar geochronology. Earth and Planetary Science Letters 121, 333–348.

Worzewski, T., Jegen, M., Swidinsky, A., 2012. Approximations for the 2-D coast effect on marine magnetotelluric data. Geophysical Journal International, 189, 357–368. doi:10.1111/j.1365-246X.2012.05385.x

Figures

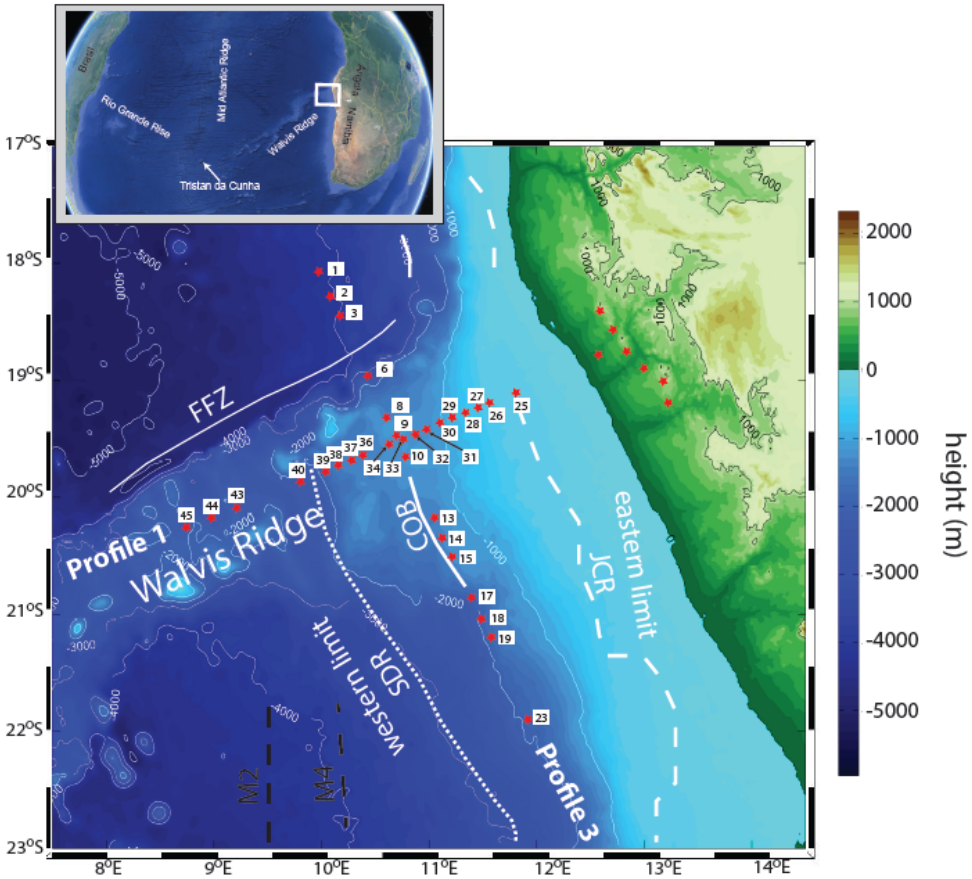

Figure 1: Experiment layout for the marine MT experiment. Inset shows the location of the experiment and labeled major geological features relevant to the paperTwo profiles (profile 1 and profile 3) were occupied by OBEM stations. Red stars and numbers mark stations that delivered data of sufficient quality to be included in the inversion. Overlain are labelled geological features from Gladzenko et al. (1998) in white: The Floreanopolis Fracture Zone (FFZ) (Sibuet et al., 1984), the continent-ocean boundary COB, the western end of SDR sequences (dotted line) and the eastern border of the Jurassic-Creataceous Rift Basin (JCR, dashed line). The eastern bound of the SDR sequence and western bound of the JCR coincide with the COB.

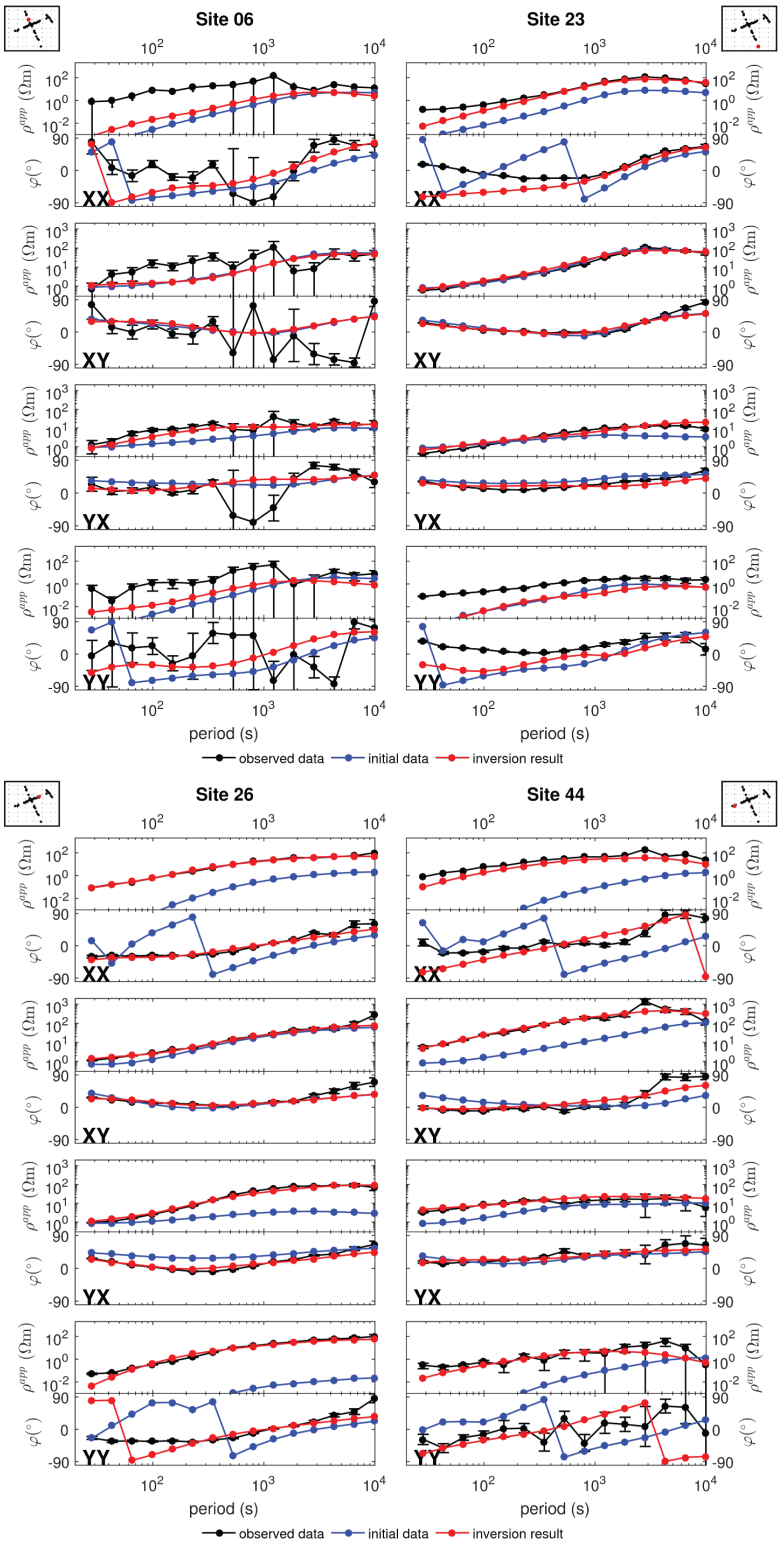

Figure 2: Apparent resistivities and phases for few exemplary measurement sites. The chosen sites represent data with moderate quality (left panel) and good quality (right panels) for all four elements of the impedance tensor. Black curve show the observed data. Modeled data based on the starting model (initial data) are depicted as blue lines. Red lines show the predicted data of the final inversion model presented here.

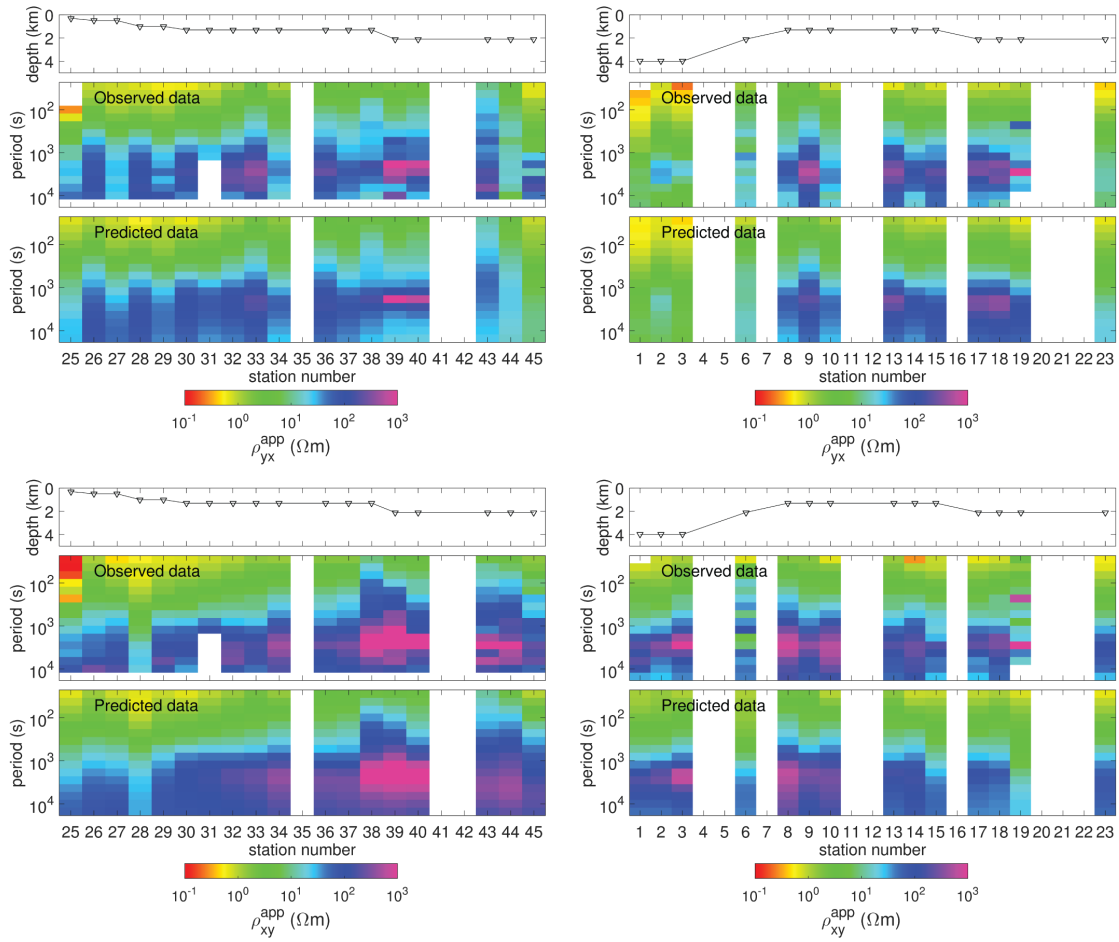

569

570 Figure 3: Comparison of predicted and measured off-diagonal elements of the
571 impedance tensor given as apparent resistivity and phase for sites along Profile 100
572 (along Walvis Ridge) on the left and Profile 3 (across Walvis Ridge) on the right.

573

574

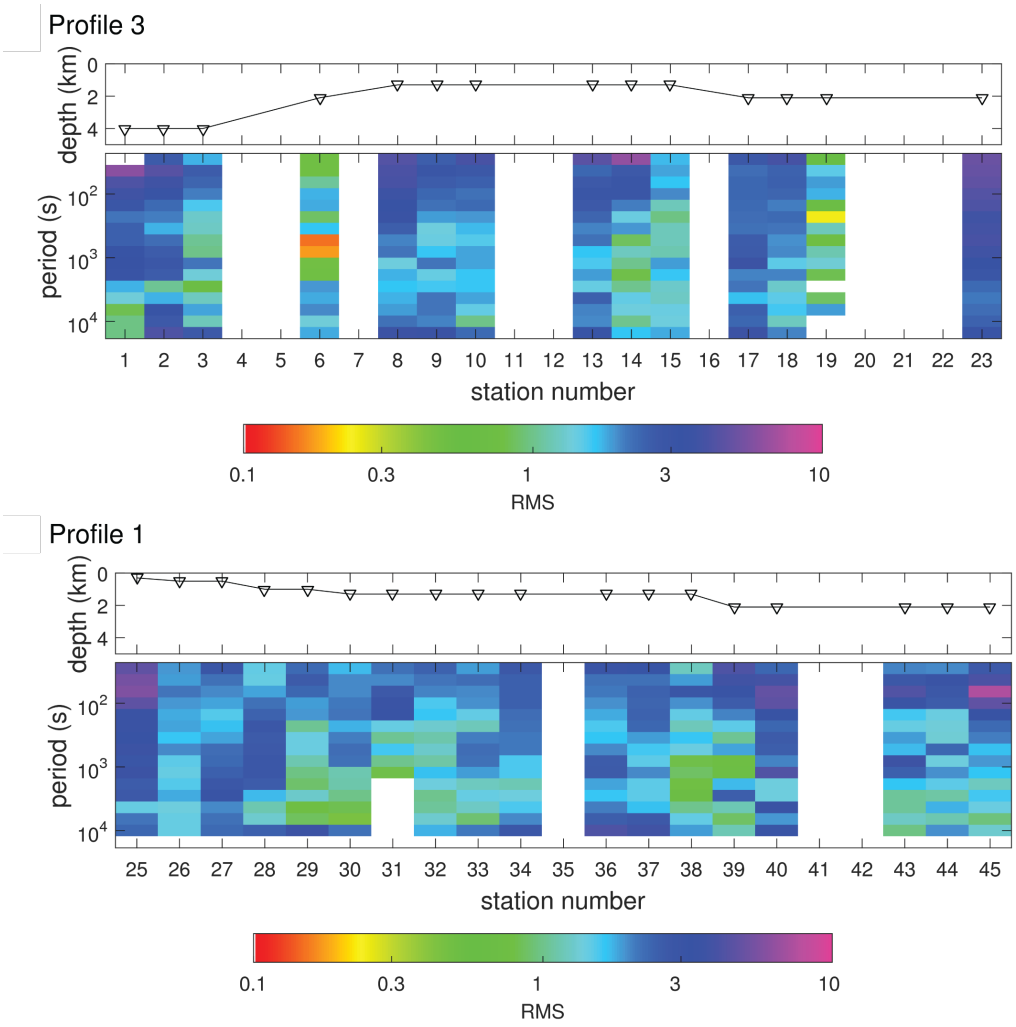

575

576 Figure 4: RMS misfit distribution between observed and predicted impedance values for
577 profile 3 (upper panel) and profile 1 (lower panel). The RMS was calculated at each site
578 and frequency based on the sum of the individual RMS for each impedance matrix
579 element. For the calculation we assumed a constant error given by the maximum error of
580 the impedance elements at this site and period.

581

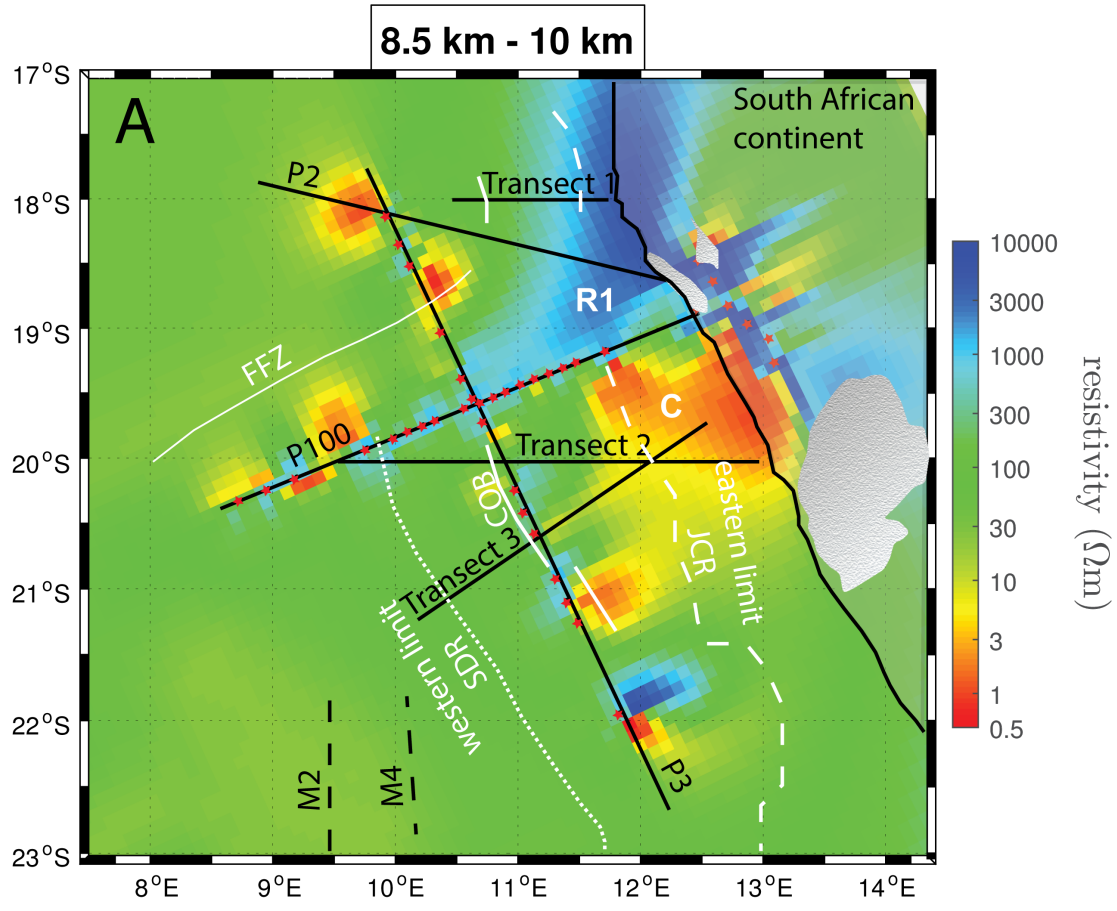
8.5 km - 10 km
A
South African continent
P2
Transect 1
R1
FFZ
P100
C
Transect 2
COB
Transect 3
JCR
eastern limit
SDR
western limit
M2
M4
P3
17°S
18°S
19°S
20°S
21°S
22°S
23°S
8°E
9°E
10°E
11°E
12°E
13°E
14°E
10000
3000
1000
300
100
30
10
3
1
0.5
resistivity (Ωm)

582

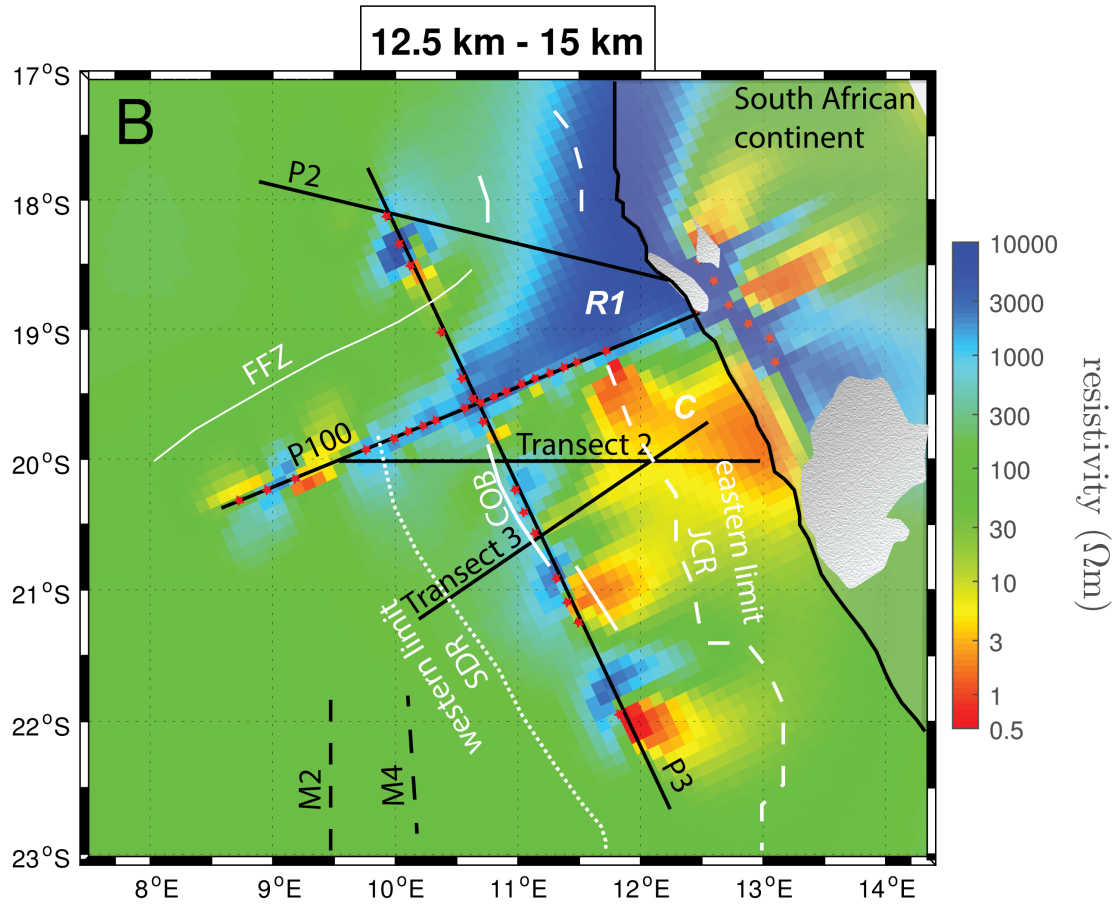
12.5 km - 15 km
B
South African continent
P2
R1
FFZ
P100
C
Transect 2
COB
Transect 3
JCR
eastern limit
SDR
western limit
M2
M4
P3
17°S
18°S
19°S
20°S
21°S
22°S
23°S
8°E
9°E
10°E
11°E
12°E
13°E
14°E
10000
3000
1000
300
100
30
10
3
1
0.5
resistivity (Ωm)

583

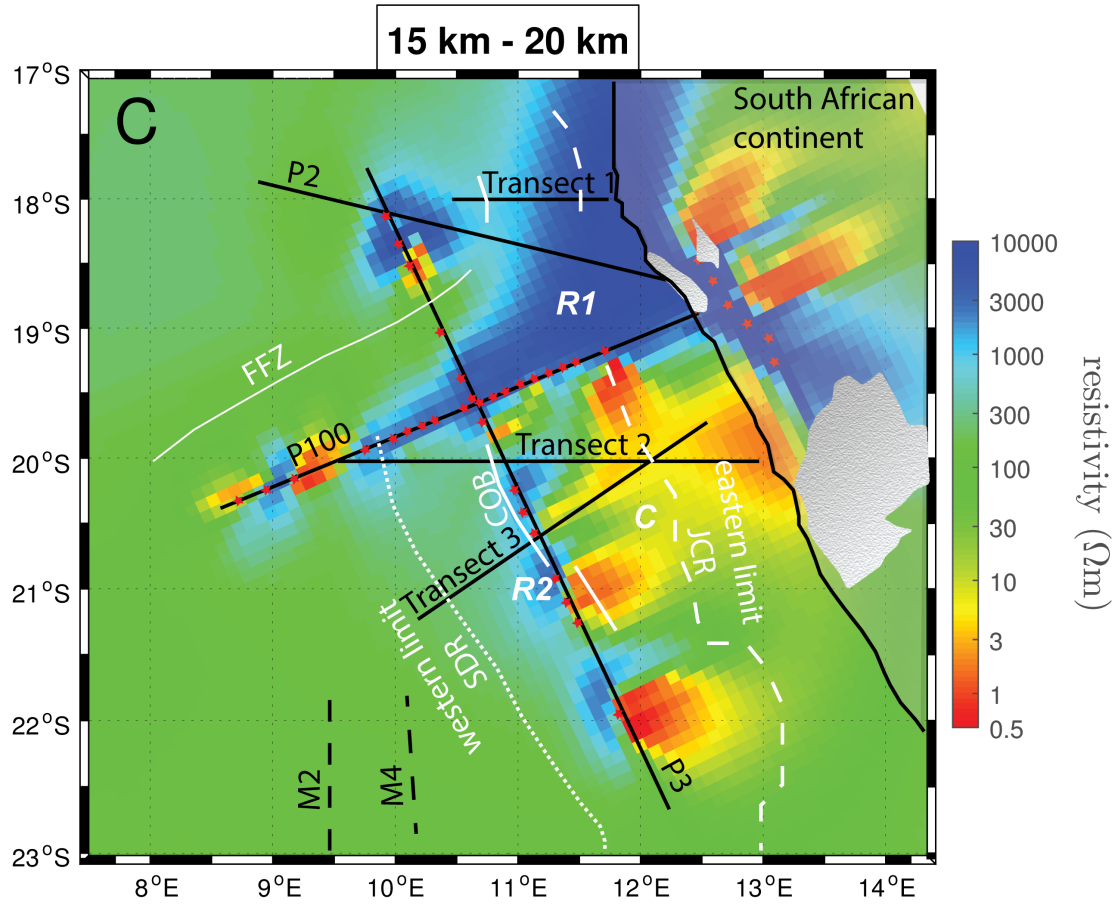
15 km - 20 km
C
South African continent
P2
Transect 1
R1
FFZ
P100
Transect 2
COB
Transect 3
R2
C
JCR
eastern limit
SDR
western limit
M2
M4
P3
17°S
18°S
19°S
20°S
21°S
22°S
23°S
8°E
9°E
10°E
11°E
12°E
13°E
14°E
10000
3000
1000
300
100
30
10
3
1
0.5
resistivity (Ωm)

584

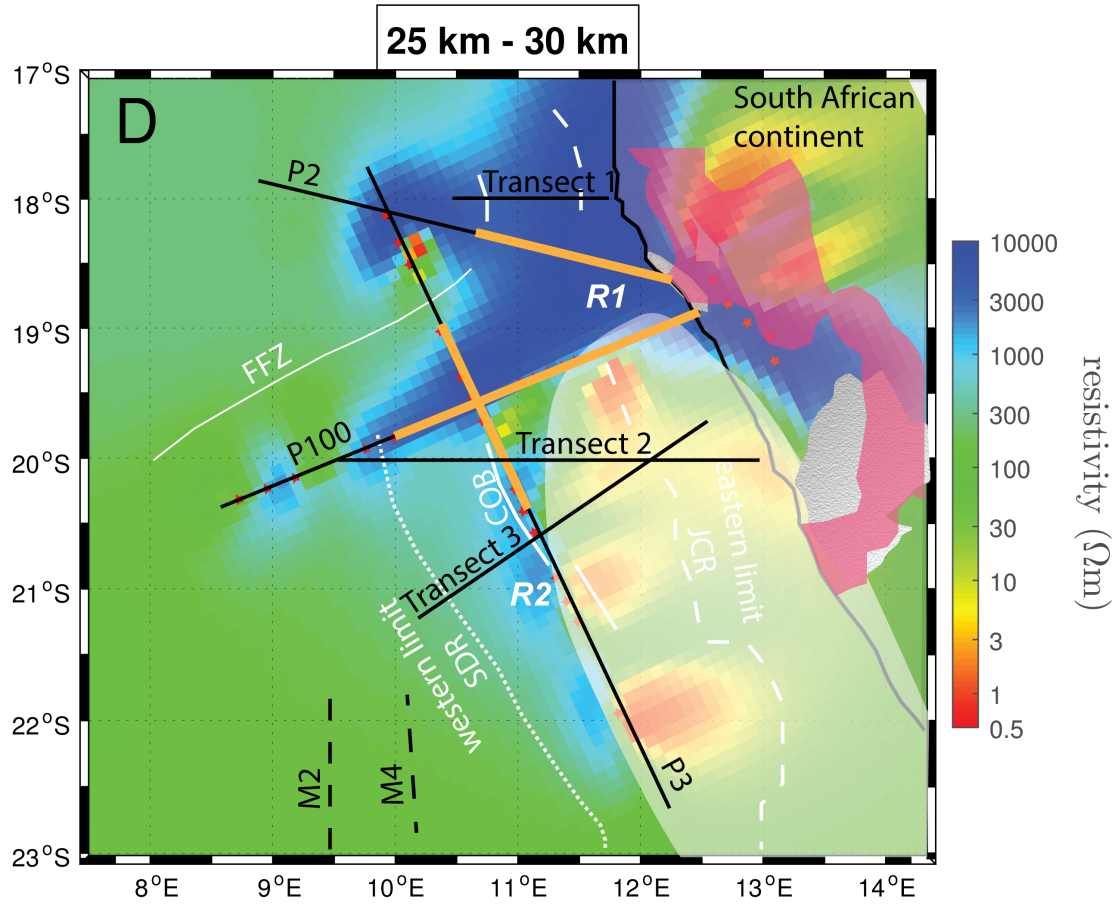
25 km - 30 km
D
South African continent
P2
Transect 1
R1
FFZ
P100
Transect 2
COB
Transect 3
R2
JCR
eastern limit
SDR
western limit
M2
M4
P3
17°S
18°S
19°S
20°S
21°S
22°S
23°S
8°E
9°E
10°E
11°E
12°E
13°E
14°E
10000
3000
1000
300
100
30
10
3
1
0.5
resistivity (Ωm)

585

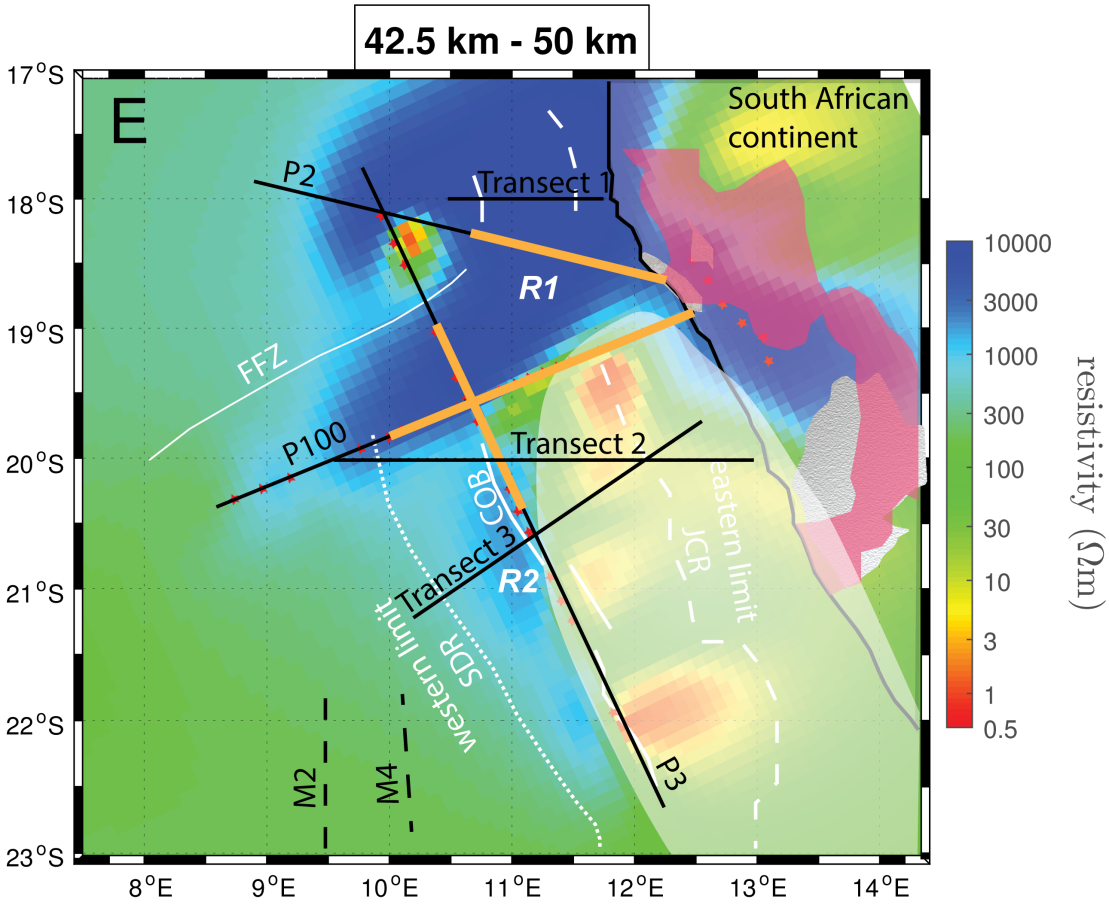

586

587 Figure 5: Areal depth slices through the resistivity model representing the derived resistivity
588 at 8.5km-10km (A), 12.5km-15km (B), 15km-20km (C), 25km-30km (D) and 42km-50km
589 (E). Overlain are labelled geological features from Gladzenko et al. (1998) in white: The
590 Floreanopolis Fracture zone (FFZ), the continent-ocean boundary COB and the western end
591 of SDR sequences (dotted line) and the eastern border of the late Jurassic-early Cretaceous
592 Rift Basin (JCR, dashed line). The eastern bound of the SDR sequence and western bound of
593 the JCR coincide with the COB. Seismic profiles from Gladzenko (transect 1 to 4) and
594 Fromm et al., 2015 (P2, P3, P100) are shown as black lines. Orange line denote the
595 underplating inferred by Fromm et al, 2015 (panels D and E). Grey textured areas show
596 region of flood basalt. Positions of MT stations used in analysis are marked by red stars. Pink
597 area shows the outline of the continental high density lower crustal body as derived by
598 Maystrenko et al., 2013 (panels D and E). Please note that the high density body is cut off in
599 the north where their study area ends. Offshore lower crustal high density bodies have been
600 omitted due to clarity of figure.

601

602

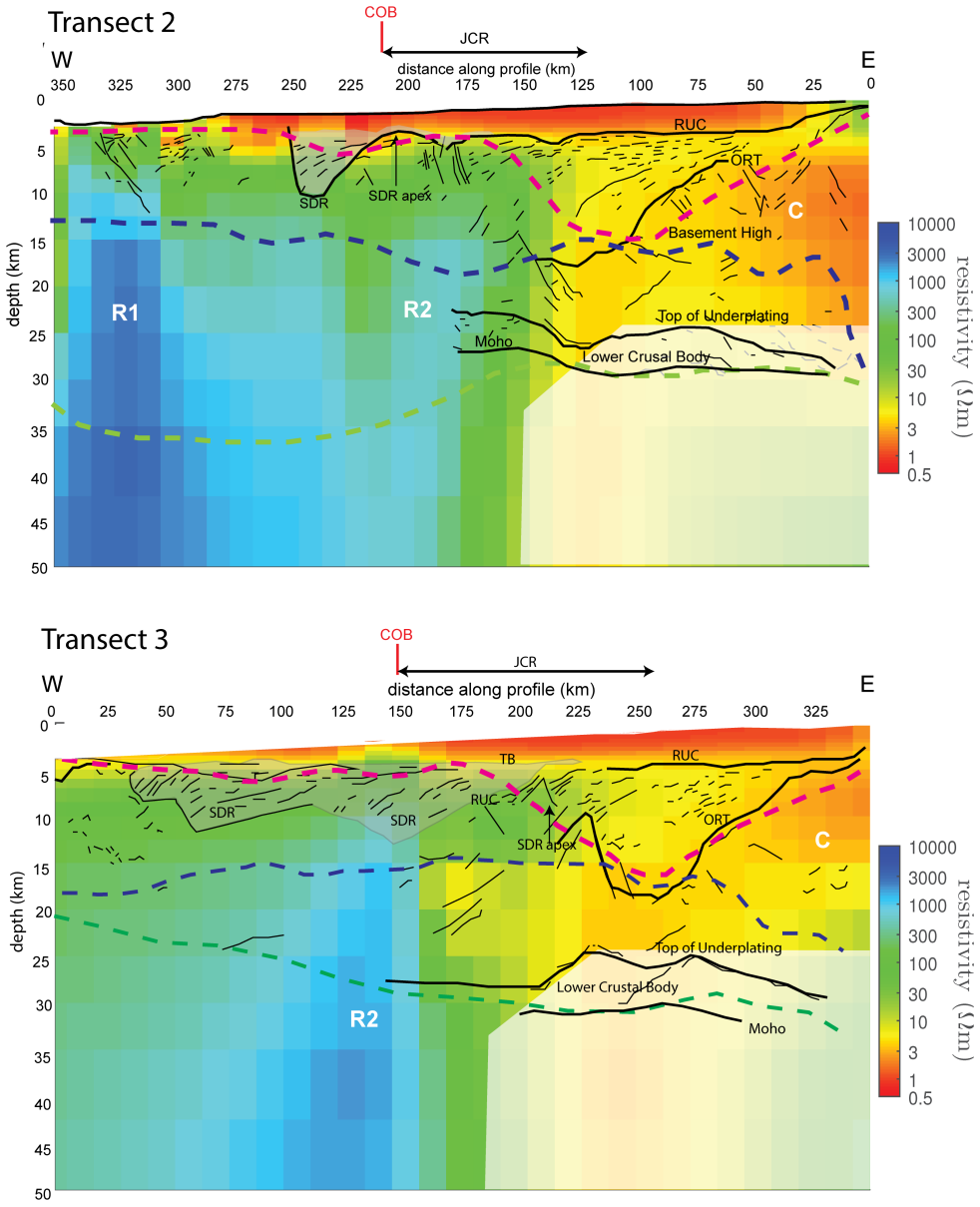

603

604 Figure 6: Comparison of resistivity model with seismic data along transect 2 (upper panel)
605 and transect 3 (middle panel). The seismic data is represented as line drawing and taken from
606 a depth section in Gladzenko et al. (1998) together with his notation of the major geological
607 features: RUC denotes the Late Jurassic – Early Cretaceous rift basin, ORT the old rift
608 unconformity, TB top basalt and SDR seaward dipping reflector. The dashed magenta, blue
609 and green line denote the base of the sediments and top of lower crustal high velocity body
610 and the Moho as derived in a gravity data study by Maystrenko et al. (2013).

611

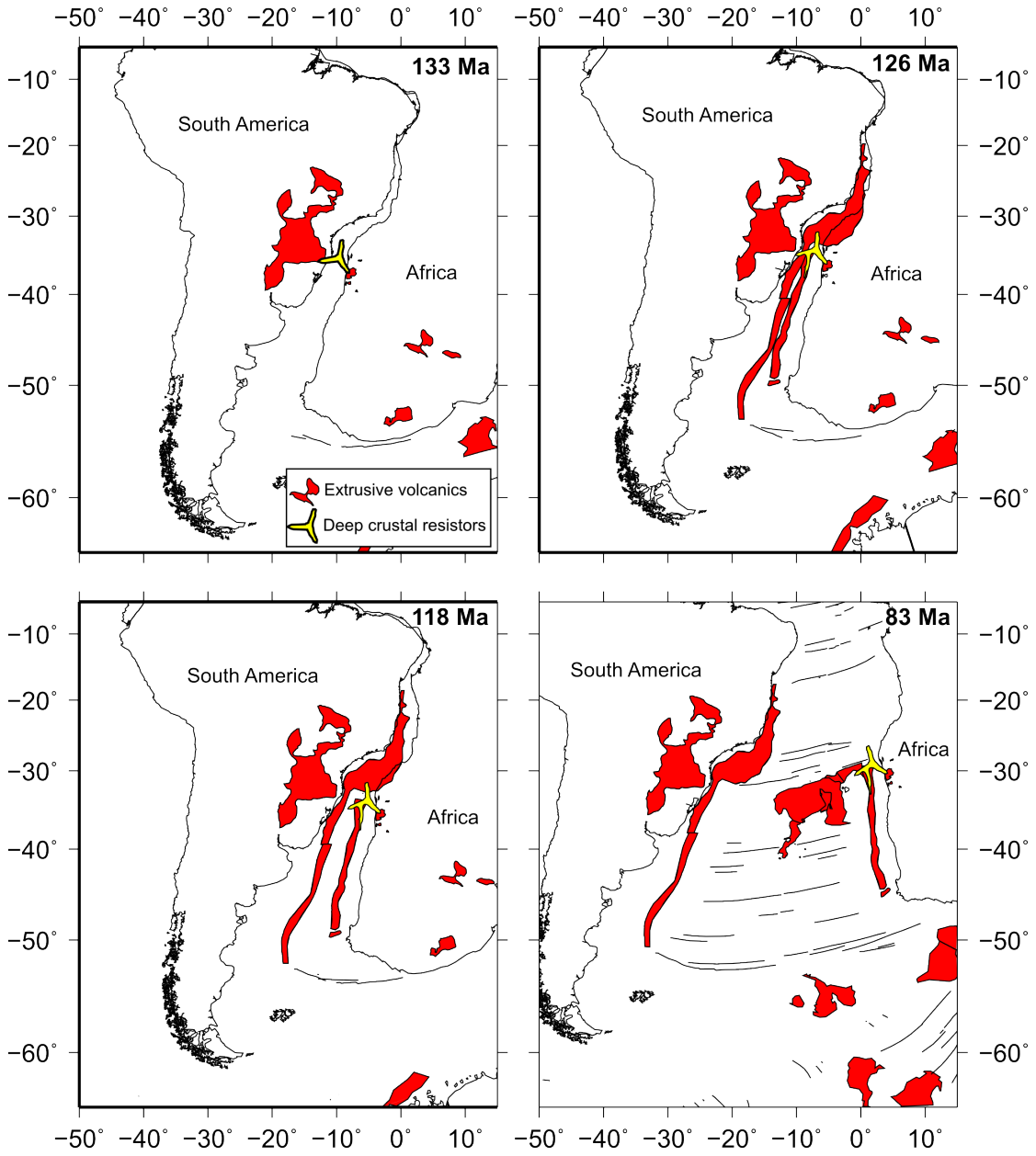

612

613 Figure 7: Plate tectonic reconstruction (Seton et al., 2012) showing the location of the high
614 resistivity anomaly through time placing the hotspot impingement underneath the African
615 Plate at 133 Ma and subsequent development of another high resistivity anomaly during the
616 emplacement of the seaward dipping reflectors between 133 Ma and 126 Ma. Outlines of
617 large igneous provinces based on Coffin and Eldholm (1994).